Title: Selection for early reproduction leads to accelerated aging and extensive metabolic remodeling in *Drosophila melanogaster* populations

Authors: David L. Hubert[1*], Kenneth R. Arnold[2], Zachary G. Greenspan[2], Anastasia Pupo[2], Ryan D. Robinson[2], Valeria V. Chavarin[2], Thomas B. Barter[3], Danijel Djukovic[4], Daniel Raftery[4], Zer Vue[5], Antentor Hinton Jr.[5], Melanie R. McReynolds[6], Benjamin R. Harrison[7], and Mark A. Phillips[1*]

[1]Department of Integrative Biology, Oregon State University

[2]Department of Ecology and Evolutionary Biology, University of California, Irvine

[3]Children's Hospital Los Angeles

[4]Northwest Metabolomics Research Center, Department of Anesthesiology and Pain Medicine, University of Washington

[5] Department of Molecular Physiology and Biophysics, Vanderbilt University, Nashville, TN, 37232, USA.

[6]Department of Biochemistry and Molecular Biology, Pennsylvania State University

[7]Department of Lab Medicine and Pathology, University of Washington

[*]Corresponding authors: David Hubert (david.hubert@oregonstate.edu) and Mark Phillips (philmark@oregonstate.edu)

Abstract

Experimental evolution studies that feature selection on life-history characters are a proven approach for studying the evolution of aging and variation in rates of senescence. Recently, the incorporation of genomic and transcriptomic approaches into this framework has led to the identification of hundreds of genes associated with different aging patterns. However, our understanding of the specific molecular mechanisms underlying these aging patterns remains limited. Here, we incorporated extensive metabolomic profiling into this framework to generate mechanistic insights into aging patterns in *Drosophila melanogaster*. Specifically, we characterized metabolomic change over time associated with accelerated aging in populations of *D. melanogaster* under selection for early reproduction compared to their controls. Using this data we: i) evaluated the evolutionary repeatability across the metabolome; ii) evaluated the value of the metabolome as a predictor of "biological age" in this system; and iii) identified specific metabolic pathways associated with accelerated aging. Generally, our findings suggest that the metabolome is a reliable predictor of age and senescence in populations that share a recent evolutionary history. Metabolomic analysis revealed that generations of selection for early reproduction resulted in highly repeatable alterations to the metabolome. Specifically, changes in carbohydrate, amino acid, and TCA cycle-related metabolite abundances over time point to metabolic remodeling that favors rapid early reproduction with long-term consequences for carbohydrate and protein utilization.

Introduction

Experimental evolution studies using genetically diverse *Drosophila melanogaster* (*D. melanogaster*) populations have been a continual source of insight into the factors that underlie differences in longevity and rates of senescence between individuals, which remain a major unresolved issue in biology. As predicted by the evolutionary theory of aging, selection for early reproduction reliably produces populations enriched for individuals that develop quickly and die young, whereas postponed reproduction has the opposite effect (Rose 1984; Luckinbill et al. 1984; Chippindale 1997; Rose et al. 2010). Studying these populations has generated insights into the physiological trade-offs associated with different aging patterns. For instance, while populations selected for early reproduction develop quickly and have high early life fecundity, they also exhibit reductions in egg viability (Chippindale et al. 1997), stress resistance (Kezos et al. 2023), lifetime fecundity, and lifespan (Burke et al. 2016). The goal of the current project is to build

on this work to better understand the molecular underpinnings of this “accelerated aging” phenotype.

Over the past decade, the combination of experimental evolution and next-generation sequencing technologies has emerged as a powerful tool for studying the genetics of complex traits. Major findings from studies that analyze quantitative traits, such as longevity, stress resistance, and body size, have consistently shown the underlying genetic architecture is complex, often involves hundreds of genes (e.g. Turner et al. 2011; Fabian et al. 2018; Tobler et al. 2015; Barter et al. 2019; Kezos et al. 2019), and many of these traits may also involve pleiotropic interactions (Greenspan et al. 2024) as well as genetic redundancy (Hardy et al. 2017; Barghi et al. 2019). Because of this inherent complexity, insights into the molecular mechanisms underlying trait variation have been modest. With respect to aging and longevity, functional conclusions are largely limited to enrichment for gene ontology terms broadly related to neurological development, immune function, and energy use and metabolism (Carnes et al. 2015; Fabian et al. 2018, Barter et al. 2019). In an effort to move beyond the finding that complex traits are highly polygenic, some have turned to metabolomics as a path forward (e.g. Phillips et al. 2022; Cavigliasso et al. 2023).

Metabolomics involves the analysis of metabolites, molecules <2000 Da, collectively referred to as the metabolome. Because metabolites constitute the functional and energetic building blocks of all life, metabolomics provides a potential link between genotype and phenotype (Harrison et al. 2020). Among the -omic layers of systems biology (e.g. transcriptome, proteome, etc.) the metabolome is thought to closely reflect organismal phenotypes (Dettmer et al. 2006; Hoffman et al. 2014). While genomic, transcriptomic, and proteomic signals can be complicated by epigenetic and posttranslational modifications, the downstream positionality of the metabolome provides a marker more representative of the observed phenotype (Patti et al. 2012). The metabolome of flies is highly dynamic with age and is sensitive to effects on longevity from environmental conditions, genetic variation, and pharmacological interventions (Avanesov et al. 2014; Laye et al. 2015; Jin et al. 2020). Zhao et al. (2022) recently used metabolomic data to build a model, primarily to predict age, but whose residual variation predicted mortality risk. This approach, colloquially referred to as a “metabolomic clock”, connects patterns of age in the metabolome to the rise in mortality risk that defines biological aging. Using these clock models could provide insight into the molecules associated with the relative pace of chronological and biological age, where the former is simply a measure of the passing of time, and the latter is a relative measure of senescence (Jylhävä et al. 2017). In an experimental evolution context, such

clock models could allow us to test hypotheses about the aging patterns that result from selection on life history (Parrott and Bertucci 2019).

Here, we applied metabolomic analysis to a set of ten replicate fruit fly populations where hundreds of generations of selection for early reproduction has led to enrichment for an accelerated aging phenotype where flies develop quickly and die young relative to controls. In effect, creating a disconnect between the chronological and biological age when compared to the ancestral population. Previous work in this system has consistently demonstrated the evolutionary repeatability of this accelerated aging signal with high levels of genomic (Graves et al. 2017), transcriptomic, (Barter et al. 2019), and phenotypic convergence (Burke et al. 2016; Kezos et al. 2023) between newly derived and long-standing populations subjected to the same selection pressures. This rapid convergence has been attributed to the idea that adaptation in these populations is primarily fueled by shifts in common genetic variants present in the ancestral population that this system was derived from.

In Phillips et al. (2022), we compared metabolomic differentiation patterns between 21-day-old individuals from the accelerated aging (A-type) populations and their controls (C-type) and found evidence of altered tricarboxylic acid (TCA) cycle activity, carbohydrate metabolism, and neurological function in the A-type populations. Because age-specific mortality rates are known to greatly diverge between the fly populations by day 21, we concluded that the observed differences in metabolic activity were a potential driver of the aging and longevity differences observed between the selection regimes. One possibility is that these differences were due to metabolic remodeling, similar to the differences between reproductive and non-reproductive flies (Koliada et al. 2020; Rodrigues et al. 2023). Such remodeling in the A-type populations could meet energetic and nutritional demands associated with fast development and early reproduction and come at the expense of somatic maintenance. However, our ability to make a definitive statement was limited as Phillips et al. (2022) included only a single age class and did not establish if this metabolomic difference reflected a difference in biological aging. In the present study, we seek to remedy this shortcoming and derive even deeper mechanistic insights by testing for accelerated biological age and characterizing how metabolomic profiles change over time in the A and C-type regimes.

We hypothesize that the metabolome is connected to the physiological tradeoffs that accompany adaptation to the A-type selection regime. If true, we predicted that i) metabolomic profiles should rapidly converge for populations subjected to the same selective pressures, and

ii) a metabolomic clock should not only capture signals of chronological age, but also reflect differences in biological age associated with the response to different selective pressures.

To test these predictions and further explore the data, we had three primary objectives:

Objective 1) To test our first predictions, we compared the metabolomes of long-standing and recently derived subpopulations subjected to the same selective pressures to evaluate levels of metabolomic convergence between them. If the known life history trade-offs that characterize the response to this selection in this system have a clear signal in the metabolome, newly derived and long-standing subpopulations should show a high degree of metabolomic convergence.

Objective 2) To test our second prediction, we created separate metabolomic clocks using data from A or C-type regimes. As with previous studies, we expect that these models will capture signals associated with age. In other studies, the residual error in the clock reflected mortality risk within the studies population. In this setting however, we use such 'clock error' to test our hypothesis about the relative biological ages of flies from these two regimes. We expect that, relative to the metabolome of the C-type populations, the A-type population metabolome will appear 'older'. Similarly, we predict that a clock model based on the metabolome of the A-type populations will predict younger biological age for the metabolome of the C-type populations.

Objective 3) To generate insights into the specific metabolomic pathways underlying the accelerated aging phenotype observed in the A-type regime, we characterized the metabolomic trajectories associated with the differently aging populations under the A and C-type selection regimes. We were primarily interested in changes related to energy metabolism and TCA cycle activity, as the significance of these pathways were previously identified. We expected to see metabolic patterns consistent with high reproductive output in early in A-type flies, followed by metabolomic patterns associated with older flies occurring in the A-type flies when compared to the C-type flies of the same chronological age.

Materials and Methods

Experimental Populations

All 20 *D. melanogaster* populations used in this study share a common origin, traced back to the large and outbred Ives (1970) population. Numerous populations have been derived from this wild-bred lineage, first by Michael Rose and Brian Charlesworth (Rose & Charlesworth 1980; Rose & Charlesworth 1981; Rose 1984) and then by generations of the Rose Lab (e.g.

Chippindale 1997, Burke et al. 2016), to study the evolutionary theory of aging. Here we focused on the A-type populations and their controls, the C-type populations (Figure 1B). A-type populations were maintained on a 10-day generation cycle, whereas the C-type populations were maintained on a 28-day cycle. As a result of this difference, the A-type populations exhibit accelerated development, reduced longevity, higher early-life fecundity, and lower stress tolerances than to the C-type populations (Burke et al. 2016; Kezos et al. 2023). There are two subpopulations within the A and C-type populations, ACO_{1-5}/AO_{1-5} and CO_{1-5}/nCO_{1-5}, respectively (See Figure 1A). Each subpopulation is distinguished by the number of generations they have been under selection, with AO and nCO having been derived more recently than ACO and CO to test questions about evolutionary repeatability (see Burke et al. 2016 and Graves et al. 2017). We know that these subpopulations have converged at several phenotypic levels and now generally treat them as replicates of the same treatment, based on previous phenotypic (Burke et al. 2016), genomic (Graves et al. 2017), and transcriptomic (Barter et al. 2019) studies. At the time of sampling for this project, the ACO and AO subpopulations had ~1,000 and ~490 generations under selection, respectively, whereas the CO and nCO subpopulations had ~415 and ~160 generations, respectively.

Mortality Assays

Adult mortality assays were based on the initial protocols outlined in Burke et al. (2016) and tested the same 20 replicate populations of ACO, AO, CO, and nCO. The progenitor stock populations were sampled on a 14-day culture cycle for two generations, staggered a day apart to align the different treatments to a shared calendar and reduce the impact of gene by environment interaction. Each population was represented by two cohorts (e.g. ACO1α & ACO1 β) of ~1,500 flies in a Plexiglas cage, supplied with fresh banana-molasses based media (as described in Phillips et al. 2018) each day with yeast solution to induce oviposition once transferred on day 14 from egg. At the same time each day, all dead flies were removed from each cage to be sexed and logged for each cohort until no living flies remained. Mortality data was pooled between cohorts to give the total number of deaths per day of each population. The Burke et al. (2016) protocol was modified for this experiment to remove the use of carbon dioxide in condensing cohorts when census densities were sufficiently low. Instead, flies within cohorts remained in the same cage for the duration of the experiment, regardless of census density. Cleaning was performed internally with hygienic tissue paper to remove waste build-up from the sides of the Plexiglas given their prolonged use.

Sample Collection

Samples were collected for metabolomic characterization using protocols described by Phillips et al. (2022). Briefly, a replicate cohort was derived for each progenitor stock population and maintained on a 14-day culture cycle for two generations, staggered a day apart to mitigate the impact of gene-by-environment interactions. Female flies were randomly drawn from the second generation from each population for metabolomic extraction. Each cohort consisted of ~1,500 flies in a Plexiglas cage and was fed fresh banana-molasses based media each day with yeast solution to induce oviposition. On each collection timepoint from initial oviposition, ~50 females were collected from each cohort, dry frozen in liquid nitrogen, and stored at −80°C prior to metabolite extraction. Due to decreased population sizes at late ages, two samples contained less than 50 flies: ACO_1 day 35 (n= 25), and nCO_4 day 70 (n= 36). The ages used to describe these populations are referenced from the time of egg deposition to collection of adults, describing the total life span of the individual, not just the time as an adult. These populations were selected based on generation cycle, not on adult age, so this frame of reference will be used throughout.

The time points used in this study were informed by demographic data and prior studies outlining unique characteristics of these regiments in either the “aging” or “non-aging” phases of their lifespan, where aging is characterized by increased mortality rates within the population (Burke et al. 2016, Barter et. al 2019). The adult female age-specific mortality distributions (Figure 2) were generated from cohorts of the ACO, AO, CO, and nCO populations undergoing the same density and diet conditions as those used for metabolomic extraction. The main distinction between the cohorts used in (Figure 2) was the daily removal of dead flies from each cage, which were logged to measure mortality patterns. We optimized our new procedure from the initial protocol detailed by Burke et al. (2016) by not measuring fecundity concurrently and by not anesthetizing flies using carbon dioxide to transfer into new cages when density dropped to 50% to reduce handling interventions.

For the A-type regime, day 9 from oviposition represents a uniquely non-aging phase of the accelerated lines whereas days 21, 28, and 35 begin rapid senesce. Conversely, the C-type regimes were sampled in parallel on the same days (21, 28, and 35), but were only expected to exhibit major aging-related declines in fitness starting at day 35 (Figure 2).

Sample Preparation

Aqueous metabolites for targeted liquid chromatography–mass spectrometry (LC-MS) profiling of 80 fly samples were extracted using previously described protein precipitation method

(Kurup et al. 2021; Meador et al. 2020). Briefly, samples were homogenized in 200 μL purified deionized water at 4 ˚C, and then 800 μL of cold methanol containing 124 μM 6C13-glucose and 25.9 μM 2C13-glutamate was added. Internal reference standards were added to the samples to monitor sample preparation. Next, samples were vortexed, incubated for 30 minutes at -20˚C, sonicated in an ice bath for 10 minutes, centrifuged for 15 minutes at 14,000 rpm at 4˚C, and then 600 μL of supernatant was collected from each sample. Lastly, recovered supernatants were dried on a SpeedVac and reconstituted in 0.5 mL of LC-matching solvent containing 17.8 μM 2C13-tyrosine and 39.2 3C13-lactate, and internal reference standards were added to the reconstituting solvent to monitor LC-MS performance. Samples were transferred into LC vials and placed into a temperature-controlled autosampler for LC-MS analysis.

LC-MS Assay

Targeted LC-MS metabolite analysis was performed on a duplex-LC-MS system composed of two Shimadzu UPLC pumps, CTC Analytics PAL HTC-xt temperature-controlled auto-sampler and AB Sciex 6500+ Triple Quadrupole MS equipped with ESI ionization source (Meador et al. 2020). UPLC pumps were connected to the autosampler in parallel and were able to perform two chromatography separations independently from each other. Each sample was injected twice on two identical analytical columns (Waters XBridge BEH Amide XP) performing separations in hydrophilic interaction liquid chromatography (HILIC) mode. While one column was performing separation and MS data acquisition in ESI+ ionization mode, the other column was equilibrated for sample injection, chromatography separation and MS data acquisition in ESI- mode. Each chromatography separation was 18 minutes (total analysis time per sample was 36 minutes), and MS data acquisition was performed in multiple-reaction-monitoring (MRM) mode. The LC-MS system was controlled using AB Sciex Analyst 1.6.3 software. The LC-MS assay targeted 361 metabolites and 4 spiked internal reference standards. Measured MS peaks were integrated using AB Sciex MultiQuant 3.0.3 software. Up to 210 metabolites and 4 spiked standards were measured across the study set, and over 90% of measured metabolites were measured across all the samples. In addition to the study samples, two sets of quality control (QC) samples were used to monitor the assay performance and data reproducibility. One QC [QC(I)] was a pooled human serum sample used to monitor system performance and the other QC [QC(S)] was pooled study samples, were used to monitor data reproducibility. Each QC sample was injected for every 10 study samples. The data were highly reproducible with a median coefficient of variation (CV) of 4.6 % over three days of non-stop data acquisition. Results from LC-MS can be found in Supplementary Table S1.

Data Processing and Normalization

The LC-MS data was filtered and normalized prior to analysis. Any metabolites with missing values were removed from the data set, and relative peak areas for the remaining metabolites were log-transformed to approximate a Gaussian distribution. Next, within sample metabolite data were mean-centered and unit-scaled to account for sample-to-sample variation. Given that the LC-MS profiling was performed in three separate batches over three days, we estimated main effects of batch (*B*) on each metabolite and corrected for these batch effects by taking the residuals of the following linear model:

$$Metabolite = B + \varepsilon$$

The final dataset consisted of 80 samples with measures for 202 metabolites (Table S2).

Objective 1: Metabolomic Convergence Within Selection Regime

We used linear mixed-effects models (LMM) to evaluate metabolomic convergence between recently derived and long-standing subpopulations. All LMM analyses were conducted using the lme4 package (Bates et al. 2015) in R (R Core Team, 2023).

Metabolomic Convergence Within Selection Regime

To evaluate the consistency of the metabolomic signal within selection regimes, we tested for convergence between recently derived and long-standing subpopulations (i.e., AO vs. ACO, and CO vs. nCO), using an LMM to compare the normalized, mean-centered metabolite abundance levels between subpopulations in the same selection regime, either A-type or C-type:

$$Metabolite = \mu + Sub + Age + (Sub \times Age) + Rep + \varepsilon$$

Where subpopulation (*Sub*), either long-standing or recently derived, and age from egg (*Age*) were treated as fixed effects and replicate population (*Rep*) as a random effect. The Benjamini-Hochberg procedure was used to control for false discovery rate (FDR) with a significance threshold of 0.01 (Benjamini and Hochberg 1995). Metabolites with a significant FDR for the subpopulation term represent metabolites with significant differences in abundance between long-standing or recently derived subpopulations (either ACO and AO, or CO and nCO) and are interpreted as not converged for that metabolite.

Objective 2: Metabolomic Clocks and the Effect of Selection Regime

Elastic Net Regression Model Analysis

We used two approaches to generate predicted ages for the flies based on the metabolome data, both of which avoid age predictions for replicates that were part of model training. The first was to generate *within-regime* predictions and the second was to generate regime-specific models to predict ages *between-regimes*. For the within-regime predictions, we used an iterative leave-one-replicate-out strategy, where, at each iteration, all four samples from one replicate were withheld. A 5-fold CV elastic net model was then trained to predict age using the metabolome data of the remaining nine replicates (n=36 samples), with elastic net penalty parameters, L1 and L2, selected from the default tuning grid to give the lowest root mean squared error (RMSE). The model from that iteration was then used to predict the ages of the held-out replicate. This procedure was repeated until all replicates had age predictions from a model that was trained on the data from the remaining replicates.

For the between-regime predictions, 5-fold CV elastic net models were trained on all data (n=40 samples) within each regime and then the ages for the opposite regime were predicted from these models. So, together, the within-regime and between-regime strategies resulted in predictions made on data that were not a part of model training. For simplicity, we refer to the between-regime models built with metabolome data from the A-type or the C-type as the A-type clock and the C-type clock. Model fitting was conducted with the elastic net regression model implemented in the glmnet package in R (Friedman et al 2023) as discussed in Zhao et al. (2022). To compare the feature importance in the A-type and C-type clocks, we used the coefficients (β) fit to each metabolite in the respective clock models. For both clocks, the elastic net penalty L1 at the lowest RMSE was >0, and so some metabolites have $\beta = 0$ and are not features in the respective clocks.

We tested the accuracy of the within-regime predictions with the coefficient of determination, R^2 (Kvalseth 1985; Alexander et al. 2015). Where y_i (i= 1, …, n) are the ages of the test set, and $\hat{y}_i$ are the predicted ages. $\overline{y_i}$ is the mean of y_i, then R^2 is calculated as:

$$R^2(y, \hat{y}) = 1 - \frac{\sum_{i=1}^{n}(y_i - \hat{y}_i)^2}{\sum_{i=1}^{n}(y_i - \overline{y_i})^2}$$

Where an R^2 closer to 1 represents a better fitting model.

To test our hypothesis that between-regime predictions will reflect accelerated or decelerated aging, we use a linear model fit by ordinary least squares.

$$predicted\ age \sim \alpha + \beta_1\ age + \beta_2\ regime + \beta_3\ age \times regime + \varepsilon$$

Where β_2 is the age-independent effect of regime, β_3 the age-dependent effect of regime, all in a model that estimates the regime-independent effect of chronological age β_1. To test our hypothesis that the accelerated aging of the A-type is reflected in its metabolome, the metabolome data from A-type was used to get predictions from the C-type clock and tested for $\beta_2>0$ and $\beta_3>0$. Similarly, to test for relative deceleration of the C-type with reference to the A-type clock, $\beta_2<0$ and $\beta_3<0$ were tested from predictions made with the A-type clock.

Objective 3: Metabolomic Trajectories of Rapid Aging

Principal Components Analysis

To determine the extent to which metabolomic profiles cluster by age and selection treatment, a principal components analysis (PCA) was conducted on the normalized, mean centered metabolomic data using the stats package (version 4.3.1) in R, and data visualization was conducted using the ggplot2 package (3.4.4) in R (Wickham, 2016).

Metabolomic Differentiation Between Populations Under Different Selection Regimes

A LMM was used to compare the metabolite levels between populations under different selection regimes, either A-type or C-type, over time to test for the effects of selection, age, and the interaction between selection and age on the normalized, mean centered data:

$$Metabolite = \mu + Sel + Age + (Sel \times Age) + Rep + \varepsilon$$

Where selection regime (*Sel*) and age from egg (*Age*) were treated as fixed effects and replicate population (*Rep*) a random effect. We used a significance threshold of FDR < 0.01. This model was compared to a larger model that accounted for differences between the long-standing populations, and the more recently derived populations (e.g. ACO, AO, etc.), using the Akaike information criterion (AIC). However, adding this term did not improve the fit of the model (see Table S3 for results). The results of the LMM were visualized as an UpSet plot made using the UpSetR package (1.4.0) in R (Conway et al., 2017). The UpSet plot depicts the number of

metabolites that were significant for each of the regression terms (FDR < 0.01), as well as the number of significant metabolites shared between any combination of the terms.

Characterizing Metabolite Abundance Patterns

To characterize metabolite abundance patterns over time and between selection regimes, we performed log2 fold change (L2FC) calculations on the normalized, mean centered metabolomic data that was further adjusted to facilitate L2FC calculation. Mean normalized, mean-centered values were computed for each metabolite ($\bar{x}$), by age (*a*) and selection condition (*s*). Adjusted mean values ($\bar{A}$) were calculated by subtracting 1.1 times the absolute value of the minimum mean for each metabolite within each selection condition ($\bar{x}_{min_s}$).

$$\bar{\mathrm{A}} = \bar{x}_{sa} - 1.1|\bar{x}_{min_s}|$$

L2FC was then calculated for each metabolite, within each selection condition, comparing the adjusted mean values for each time point sequentially in chronological order.

$$\mathrm{logFC}_{t,t'} = \log_2\left(\frac{\bar{\mathrm{A}}_{t'}}{\bar{\mathrm{A}}_t}\right)$$

Where $\bar{A}$ represents the adjusted metabolite abundance value described above, *t* represents the initial time point, and *t'* represents the next time point chronologically for each comparison. Resulting L2FC values were visualized using heatmaps consisting of metabolites of interest, and clustered by similarity. Additionally, to explore the significance in abundance changes between any two given time points for each metabolite, the normalized, mean-centered values were compared between sequential time points using a two-sample Wilcoxon signed ranked exact test, paired by population replicate, then adjusted for FDR.

Results

Objective 1: Metabolomic Convergence Within Selection Regime

Metabolomic Convergence Within Selection Regime

Using an LMM to test for convergence of the metabolome between recently derived and long-standing subpopulations under the same selection regime revealed that the majority of metabolites were converged between subpopulations, with no metabolites differing between

recently derived (AO) and long-standing (ACO) A-type subpopulations (FDR > 0.01, Table S4). Of the 202 metabolites tested, only six were found to differ between the recently derived (nCO) and long-standing (CO) C-type subpopulations (FDR < 0.01, Table S4). Of these six metabolites, proline, n-glycyl-proline, erythrose-4-phosphate, glucose 6-phosphate, and cGMP all had higher mean normalized abundance in the more recently derived nCO populations, and 1/3-methylhistidine had higher mean normalized abundance in the long-standing CO populations. Further, we did not identify any metabolites differing in age trajectory within either selection regime, as estimated by the interaction term (subpopulation x age, FDR > 0.01), showing general metabolomic convergence between recently derived and long-standing subpopulations.

Finding non-converged metabolites in only the C-type populations, which have experienced fewer generations in their selection regime relative to the A-type populations (Figure 1A), led us to further investigate the importance of selection duration and its impact on metabolomic convergence. We hypothesized that the non-converged metabolites found in the C-type populations were a result of higher variance in metabolite abundance in the newly derived populations relative to the longstanding populations, as the populations with fewer generations are perhaps still adapting and have not reached the phenotypic 'optimum' associated with that selection regime. To test this hypothesis, we conducted a Levene's test for homogeneity of variance between sub-populations of the same selection regime for each metabolite and each age using the car package (3.1-2) in R with standard settings (Fox and Welsberg 2019). Resulting p-values were converted to reflect a one-tailed test, where the tail of interest represented higher variance in the newly derived populations, and then these p-values were adjusted for FDR. Contrary to our hypothesis, no metabolites showed a higher variance at any age in the newly derived populations when compared to the long-standing populations for either regime (FDR > 0.01, Table S5).

Objective 2: Metabolomic Clocks and the Effect of Selection Regime

Metabolomic Clock Results

Within regime elastic net regression models (clocks) predicting age from the metabolome of C-type or A-type flies were accurate, with an R^2 of 0.955 and 0.886 respectively (Figure 3). To test hypotheses about the differences in biological age, or the pace of aging in response to selection, we first fit a linear model to test for effects of chronological age on the predictions the C-type clock when applied to flies from the A-type (Methods, Figure 3A). We found a significant regime-independent effect of chronological age ($\beta_1 = 0.95$, $p < 8.2\text{x}10^{-19}$), consistent with a

common signal from chronological age in the metabolome of both A and C type flies. The age-independent effect of selection regime was also significant (β_2 = 29.4, $p < 9.4\text{x}10^{-10}$), indicating that, relative to the C-type clock, A-type flies appeared approximately 30 days older than their actual chronological age. The age-dependent effect of selection regime (β_3 = 0.076) was not significant ($p > 0.5$). Together these results suggest that, as estimated by the C-type clock, the A-type metabolome shows a consistently greater predicted age (β_2), and no difference in the slope of the aging trajectory (β_3 = 0.076).

We then used the A-type clock to predict age in C-type flies by applying the same linear model framework to estimate the effect of selection regime on age and aging in the metabolome. The linear model term for the regime-independent effect of chronological age was significant ($\beta_1 = 0.83$, $p < 1.4\text{x}10^{-15}$), showing that the A-type clock detects increasing age in both populations. The predictions of C-type age from the A-type clock however showed a striking difference in the trajectory of predicted age over chronological age (Figure 3B). Predicted age was accurate in both A and C-type flies at the youngest age surveyed in both regimes (21 days from egg), However, at later ages the predicted ages of C-type flies were lower than their chronological age (Figure 3B). This pattern manifest as a difference in slopes, β_3 = -0.51 ($p < 3.4\text{x}10^{-8}$), and a counter-intuitive difference in the intercept term β_2 = 7.8 ($p < 8.7\text{x}10^{-4}$).

The A-type and C-type clocks make different age predictions on metabolome data from the two regimes sampled at the same chronological age. And yet, in both regimes, the two clocks predict increasing biological age as chronological age increases. We considered two possibilities, one, that the two clocks are primarily utilizing variation in the same subset of metabolites within either regime to make age predictions. Alternatively, the A- and C-type clocks could gain predictive power from two different sets of metabolites as they vary with age within-regime. To distinguish these two possibilities, we examined the coefficients fit to each metabolite within both clocks.

Both clocks used an elastic net penalty L1>0, and so at least some metabolites were given no importance. This left 50 metabolites selected as model features for the A-type clock, and 18 metabolites as model features for the C-type clock (Table S6). Of these features, eight metabolites were common to both clocks (Figure 4A). An intersection of eight metabolites, does not indicate enrichment of metabolites among the two clocks (Fisher's test, odds ratio=2.69, P=0.081). However, the coefficients for the eight metabolites common to both clocks were highly correlated (Figure 4B). In comparison to the importance (β) of the metabolites specific to the C-type or A-

type clocks, the eight common metabolites were not significantly more or less important within either clock (Figure 4C).

Objective 3: Metabolomic Trajectories of Rapid Aging

Metabolomic Profiles Are Shaped by Selection

Of the 361 targeted metabolites, 210 were detected during LC-MS profiling. Of those metabolites detected, 202 had values for all samples (see Table S7 for full details). Principal components analysis revealed clustering by both selection regime and age (Figure 5A). Apart from the 70-day-old samples from C-type populations, the A-type and C-type populations showed separation along both PC1 and PC2. The 9-day-old samples from A-type populations clustered separately from all other samples along both PC axes, showing a greater degree of differentiation for these samples than the rest. The 70-day-old samples from C-type populations were the only samples that clustered more closely with the opposing selection type, showing overlap with samples from the A-type populations at ages 28- and 35-days-old. Samples from the common ages (21, 28, and 35 days) clustered within selection regime, with some separation by age within their respective selection regimes. Additional PCs were explored but were uninformative. These patterns were consistent when subpopulation (recently derived or long-standing) was factored, and no additional differences were observed (Figure S1)

Next, an LMM approach was used to characterize specific patterns of metabolite differentiation (Table S7). Of the 202 metabolites in our data set, a total of 174 unique metabolites were identified as significant for at least 1 term (FDR <0.01) (Figure 5B). The selection term explained most of the difference in the metabolome, accounting for 115 of the 174 significant metabolites, 24 of which were unique to the term. The age term accounted for 108 significant metabolites, with 15 unique to the term. The interaction term accounted for 97 of the significant metabolites, with 24 unique to the term.

Different rates of aging associated metabolic remodeling in A and C-type populations

We uncovered several patterns by calculating L2FC for relative metabolite abundance changes within each selection regime over time. We have highlighted a few key patterns of interest (Figure 6). Additionally, the relative normalized, mean centered abundance levels for these metabolites are depicted in Supplementary Figures S2-4, and full L2FC results can be found in Supplementary Table S8. Full results from the two-sample Wilcoxon signed ranked exact test can be found in Supplementary Table S9. The key observed trends are described in the

proceeding sections. The values listed represent the median L2FC ($\tilde{X}_{FC}$) and the interquartile range (IQR) for the subset of metabolites discussed. Here, metabolomic change is divided into three relative age classes, early (1st to 2nd time points), middle (2nd to 3rd time points), and late (3rd to 4th time points).

Carbohydrate Metabolism

There was a clear pattern concerning carbohydrate abundances in the A-type population (Figures 6 and S2). There was a sharp increase in abundance for the early age class ($\tilde{X}_{FC}$ = 3.54, IQR = 0.61), stability at middle age ($\tilde{X}_{FC}$ = -0.01, IQR = 0.57), and continued stability or slight decrease at late age ($\tilde{X}_{FC}$ = -0.82, IQR = 0.83). In contrast, the carbohydrate abundances observed for the C-type populations showed a much less uniform trend, characterized by a much smaller increase in abundance for most carbohydrates at early and middle ages ($\tilde{X}_{FC}$ = 0.15, IQR = 0.82), followed by a less uniform, but generally larger change in carbohydrate abundance at late age ($\tilde{X}_{FC}$ = -2.88, IQR = 5.25). This pattern of carbohydrate abundance suggests that there is a high use of carbohydrates in 9-day-old A-type populations when the abundance is low, followed by a dramatic decrease in the use of carbohydrates as they accumulate at earlier ages. These metabolites include the "*Carbohydrate*" subset found in Table 1B.

Amino Acid Metabolism

We found three major patterns when looking at changes in amino acid abundance within each selection regime over time (Figures 6 and S3). The first pattern showed a slight decrease in abundance at early age for the A-type populations ($\tilde{X}_{FC}$ = -0.73, IQR = 0.39), which further decreased at middle age ($\tilde{X}_{FC}$ = -1.78, IQR = 0.60), continuing to decrease in abundance into late age ($\tilde{X}_{FC}$ = -2.00, IQR = 0.68). In contrast, the C-type populations showed relative stability or a slight decrease in abundance for these same amino acids from early through middle age ($\tilde{X}_{FC}$ = -0.56, IQR = 0.64), with levels decreasing steeply at late age ($\tilde{X}_{FC}$ = -3.54, IQR = 0.81). The continued decrease in abundance of these amino acids suggests either an increase in amino acid catabolism or a decrease in generation associated with age. This decrease occurred faster in A-type populations, suggesting an acceleration of this process is associated with selection for early reproduction. These metabolites include the "*Amino Acid 1*" subset found in Table 1A.

In the second pattern associated with amino acids, A-type populations showed a slight decrease in relative metabolite abundances in early age ($\tilde{X}_{FC}$ = -0.60, IQR = 0.42), a much larger decrease in middle age ($\tilde{X}_{FC}$ = -3.40, IQR = 0.01), followed by an increase at late age ($\tilde{X}_{FC}$ = 1.49, IQR = 1.24). On the other hand, we observed a large increase in relative abundance of these

metabolites in the C-type populations at early age ($\tilde{X}_{FC}$ = 4.19, IQR = 0.10), followed by a general stabilization of abundance levels through middle age and into late age ($\tilde{X}_{FC}$ = - 0.04, IQR = 0.35). This pattern differs completely between A and C-type populations, suggesting an initial high rate of amino acid catabolism in A-type populations, followed by either a decrease in use or an increase in production at the later ages. In contrast, the continual increase in amino acid abundance over time in C-type populations suggests a very different pattern of use resulting from selection. These metabolites include the "*Amino Acid 2*" subset found in Table 1A.

The third pattern associated with amino acids showed the A-type populations had a large increase in relative metabolite abundance at early age ($\tilde{X}_{FC}$ = 4.21, IQR = 0.32), typically followed by a slight decrease in relative abundance at middle age that was maintained to the late age class ($\tilde{X}_{FC}$ = -0.37, IQR = 1.33). The C-type populations showed a much more varied pattern, with no apparent synchronization when compared to A-type populations. The abundance pattern of these amino acids exhibited by A-type populations is very similar to the abundance patterns of carbohydrates for the same individuals, which suggests that these were likely used at a much higher rate in 9-day-old flies but accumulated as they were used less at older ages. These metabolites include the "*Amino Acid 3*" subset found in Table 1A.

TCA Cycle

The pattern in relative abundance of TCA cycle metabolites showed a large difference when compared between selection regimes (Figures 6 and S4). The A-type populations showed two distinct patterns, the first was a strong increase in relative abundance of the metabolites; alpha-ketoglutaric acid and PEP at early age ($\tilde{X}_{FC}$ = 4.05, IQR = 0.46), followed by general stabilization through middle age into late age ($\tilde{X}_{FC}$ = 0.10, IQR = 0.31). This abundance pattern for TCA cycle metabolites matched the carbohydrate abundance patterns, with apparent high use in 9-day-old flies followed by accumulation with age. The C-type populations did not show synchronized abundance levels for these metabolites. These metabolites include the "*TCA Cycle 1*" subset found in Table 1C.

The second pattern showed A-type flies had a strong decrease in relative metabolite abundance in early age ($\tilde{X}_{FC}$ = -3.45, IQR = 2.20), followed by a large increase in middle age ($\tilde{X}_{FC}$ = 2.32, IQR = 1.02) and then a general stabilization at late age ($\tilde{X}_{FC}$ = -0.005, IQR = 0.72). In contrast, the C-type populations showed increased metabolite abundances at early age ($\tilde{X}_{FC}$ = 1.05, IQR = 0.86) which continued to increase into middle age ($\tilde{X}_{FC}$ = 0.18, IQR = 0.17), followed by a steep decline at late age ($\tilde{X}_{FC}$ = -2.83, IQR = 3.07). The high abundances of these TCA cycle

intermediate metabolites in 9-day-old flies coupled with the low carbohydrate abundance points to high rates of energy use at day 9, followed by an accumulation as the overall metabolism slowed with age. These metabolites include the "*TCA Cycle 2*" subset found in Table 1C.

Discussion

Objective 1: Metabolomic Convergence Within Selection Regime

As previously stated, adaptation in response to selection on reproductive timing in this system is associated with a number of physiological and developmental tradeoffs with complex genetic underpinnings. Because the metabolome constitutes the functional building blocks, and energetic currency of cells, we hypothesize that the physiological tradeoffs associated with the accelerated aging phenotype of A-type flies would be reflected in the abundancies of metabolites. Alternatively, the metabolome could associate with a wide variety of traits, only some of which are involved in the accelerated development or reduced longevity that evolve under these regimes. If our hypothesis is true, then we expect that subpopulations under the same selection regime would show evidence of convergence within the metabolome, even in more recently selected subpopulations. To test this prediction, we compared the metabolomes of recently derived and long-standing subpopulations under the same selection regime. Generally, we found convergence between recently derived and long-standing subpopulations under the same selection regime, with complete convergence of the metabolome for the A-type subpopulations, and nearly complete convergence for the C-type subpopulations across age classes. Whereas all surveyed metabolites appeared converged among recently derived A-types, the newly derived (nCO) and the long-standing (CO) subpopulations showed a small number of metabolites (6) that were not converged among these subpopulations. Overall, the high levels of metabolomic convergence within selection regimes, especially for A-type populations, shows that the metabolome is a reliable biomarker of the underlying physiological responses to selection.

The difference in metabolomic convergence between selection regimes may be a result of the longer generation time experienced by the C-type selection regime (28 days) compared to the A-type selection regime (10 days), which has resulted in C-type populations experiencing less than half the number of generations under selection comparatively. The metabolites that were not converged between C-type subpopulations show similar abundance patterns at all but the oldest age (70 days from egg), at which point the abundance levels differ between subpopulations. If the differences in convergence were due to selection duration, we would expect to see corresponding

differences in metabolite variance, though when assayed, the overall variance in abundance did not differ between recently derived and long-standing populations. Alternatively, with the non-converged metabolites involved in processes such as stress response, energy use, and signaling, differences at old age may be indicative of an alternate antagonistic pleiotropic response to the selection pressures experienced by C-type. However, the number of non-converged metabolites was small relative to the number of converged metabolites, suggesting that these non-converged metabolites are not representative of the general trend observed.

Objective 2: Metabolomic Clocks and the Effect of Selection Regime

Over the lifespan of the fly, the dynamics of the metabolome have been used to connect advancing chronological age to the rise in mortality risk that defines biological aging (Zhao et al. 2022). Multivariate age prediction models (clocks), particularly epigenetic clocks, have been used to predict age across species (Meyer and Schumacher 2024; Lu et al. 2023). The use of clock models to understand the evolutionary process however is just beginning (Parrott and Bertucci 2019). Here we apply clock models of the metabolome to test our hypothesis that the rapid response to selection for early life reproduction is associated with the same underlying aging processes that are reflected in the metabolome. If true, the response to selection seen in the metabolome likely reflects shifts in physiological processes that are a part of normal aging in the ancestral population. If the rapid and repeatable shifts in allele frequency (Graves et al. 2017), and both transcriptomic (Barter et al. 2019) and phenotypic (Burke et al. 2016; Kezos et al. 2023) convergence are an indication of selection acting on common physiological mechanisms, then the components of the metabolome most closely tied to aging physiology should respond similarly. A critical prediction of our hypothesis is that the relative biological age of flies under the A-type selection regime should appear ‘older’ than flies under the C-type selection regime.

To test this hypothesis, we first trained age prediction models *within* each regime, resulting in an A-type clock and C-type clock. Both clocks captured the monotonic increase in chronological age within each respective population, with accuracy R^2 exceeding >0.88 (Figure 3). In between-regime predictions, the C-type clock detected both the chronological age increase in the A-type flies, but also a strong age-independent increase in biological age of nearly 30 days (Figure 3A). Consistent with our predictions, the C-type clock detected an increase in biological age associated with the A-type selection regime. The C-type clock did not predict an age-dependent difference between the regimes, indicating that, relative to the metabolome change in the C-type, the A-type and C-type appear to age at the same rate, despite the A-type flies appearing to be older. In fact, the C-type clock predicted even the youngest A-type samples (9 days from egg) to be ~40 days old, an age where C-type populations begin to exhibit increased mortality rates, suggesting that A-type flies show a signal of senesce at all age classes.

The A-type clock detected a biological age *increase* in C-type flies, at least early in life as reflected by the intercept term β_2 (Figure 3B), which seems to contradict our expectations. However, we lack the data prior to day 21 in the C-type populations to evaluate this possibility, and adult flies eclose from pupae only after 14 days, making pre-adult stage predictions difficult to interpret. Instead, we consider the intercept term an artifact of the significant difference in rate of aging, captured by the slope term β_3, which is highly significant. To the extent that the rise in predicted age over chronological age reflects the pace of aging (Zhao et al. 2022), the C-type populations appear to age at a slower rate in reference to the aging trajectory captured in the A-type clock (Figure 2B).

The A-type clock achieved an accuracy of R^2=0.886 when predicting age in the A-type, while utilizing only 24.8% of 202 metabolites, and the C-type clock utilized only 8.9% to achieve even higher accuracy R^2=0.955. Independently fit to two different data, the C-type and A-type clocks utilized non-intersecting metabolites, however they both included eight intersecting metabolites (Figure 4A, Table S6). While this number of intersecting metabolites is not more than expected by chance, the coefficients fit to these metabolites in both clocks were highly correlated, indicating a common axis of variation with age in the metabolome. We note that, while correlated, the coefficients fit from the A-type clock tend to be smaller than those of the C-type clock (Figure 4C). This seems to reflect the relative pace of aging in these two populations. The larger coefficients fit to predict age in the more slowly aging C-type populations could result in higher predicted ages when predicting age on the A-type metabolome.

It is important to note that, while the metabolites identified by the clock models shed light on the underlying metabolome variation related to age and to aging, elastic net and other regularized regression methods are designed in part to reduce the influence of co-linear predictors (Zou and Hastie 2005; Bujak et al. 2016). Because of this, the set of metabolites most influential in clock models may not include metabolites that share very similar age-related variation in abundance, and so do not give a complete picture of age-associated metabolome variation in which collinearity is common (Lassen et al. 2023; Avanesov et al. 2014). In this light, we turn to a descriptive analysis of the metabolome variation and its convergence within regime to describe the patterns of variation under these selection regimes.

Objective 3: Metabolomic Trajectories of Rapid Aging

To discuss the implications of the differences in metabolite abundance between selection regimes and across time, we must make assumptions about how metabolite abundances relate to the activity of specific metabolic pathways. For example, we could assume that increased abundance of a metabolite indicates increased activity of the pathway that produces it. However, as metabolites are often involved in multiple pathways – both as substrate and product – reality is likely more complex. Other factors like differences in age-specific feeding rates can also impact

abundances in ways that confound interpretation of abundances. As such, we primarily see the following work as hypothesis generating for future studies (e.g., flux assays to test hypotheses about metabolite utilization and pathway activity).

Metabolic Remodeling Facilitates Early Reproduction in the A-type Populations

In the A-type populations, we observed an increased abundance of carbohydrates after the initial day 9 timepoint suggesting a major switch in carbohydrate use as flies move past their primary reproductive window. This is generally consistent with previous studies that have shown glycolytic activity decreases with age in *D. melanogaster*, which is thought to be associated with either a shift away from utilizing carbohydrates as a primary energy source or an overall metabolic reduction (Sarup et al. 2012; Hoffman et al. 2014; Ma et al. 2018; Wang et al. 2022). Our results show this shifted pattern happened much faster in the A-type populations compared to the C-type controls at common ages. In the context of the A-type selection regime, the early carbohydrate use is likely explained by the findings of Carvalho-Santos et al. (2020), which demonstrated that experimental disruption of glycolysis during reproduction in female *D. melanogaster* revealed a cellular metabolic reprogramming that increased glycolytic activity needed for egg production. A-type populations were selected to reproduce at a very early age, with a 10-day generation cycle leaving them with approximately 24 hours post eclosion for egg production. In contrast, C-type populations have a 28-day generation cycle that allows 14 days post eclosion to produce the eggs used for the next generation.

In addition to a dramatically shorter period to produce eggs, previous fecundity assays comparing A-type and C-type populations revealed higher acute fecundity in A-type flies, with the average number of eggs laid per female more than double that of the C-type populations during their respective egg collection windows (Burke et al. 2016). The resulting rapid oviposition and increased fecundity during the reproductive window has likely resulted in selection for increased glycolytic activity to support greater and more rapid egg production at early ages in A-type populations. We plan to test this hypothesis by conducting an experiment to elucidate the specific fate and turnover of glycolytic components in these populations using stable isotope tracing.

Long-term Metabolic Dysregulation

Early glycolytic activity appears to come at the cost of subsequent glycolysis dysregulation during post-reproductive ages (21-35 days) in A-type populations. Although initially low carbohydrate abundances in 9-day-old A-type flies compared to later age A-type samples can be explained by the accelerated reproductive output, these carbohydrate abundances remain low

when compared to C-type populations at common ages. This altered pattern of metabolite abundance suggests a persistent selection-based difference in carbohydrate metabolism, potentially signaling early metabolic dysregulation in A-type populations similar to age-dependent metabolic dysregulation found previously (Sarup et al. 2012; Hoffman et al. 2014; Wang et al. 2022; Zhao et al. 2022). General glycolytic dysregulation detrimentally impacts overall health (Ma et al. 2018; Oka et al. 2021), potentially contributing to the reduced lifespan exhibited in A-type populations (Burke et al 2016). The distinct patterns of carbohydrate abundance exhibited by the A-type populations is indicative of a coordinated response that further supports the evolutionary repeatability of this selection regime illustrated by the metabolomic convergence presented earlier. While uncovering the exact mechanism behind this metabolic shift will require further investigation, this potential metabolic tradeoff between early reproduction at the cost of longevity in the A-type populations appears to be a clear example of antagonistic pleiotropy, where a trait that improves fitness at younger ages reduces fitness at older ages (Williams et al. 1957; Austad and Hoffman 2018).

Amino Acid Catabolism

The observed accumulation of carbohydrates from day 9 to day 21 in A-type flies coincided with a decrease in amino acid abundance as A-type flies age, suggesting a potential switch in energy substrates from carbohydrate to amino acid metabolism. This metabolic reprogramming associated with aging has been found in several previous studies (Hoffman et al. 2014; Ma et al. 2018; Wang et al. 2022). In a recent example, Wang et al. (2022) used stable isotope tracing and found that glycolytic function decreased with age, whereas amino acid metabolic activity (specifically serine and purine metabolism) increased with age in *D. melanogaster*. This apparent age-dependent metabolic reprogramming is not limited to *D. melanogaster*, as decreased glycolysis and increased amino acid catabolism are associated with longevity across taxa (Houtkooper et al. 2011; Weimer et al. 2014; Castro et al. 2022).

Interestingly, a recent study showed that fruit fly larvae raised on nutrient-poor diets increased amino acid catabolism as an alternative to glycolysis when resources were limited (Cavigliasso et al 2023). A reduction in glycolytic activity could create metabolic conditions similar to nutrient-poor environmental conditions, necessitating a shift to amino acid catabolism as a strategy to overcome glycolytic dysregulation. This would explain the decrease in amino acid abundance that coincides with the increase in carbohydrate abundance observed in A-type populations at ages post-reproductive selection despite the quality of food remaining unchanged.

TCA Cycle Activity

Similar to Phillips et al (2022), we found altered TCA cycle metabolite abundances in 21-day-old A-type flies when compared to C-type flies of the same age. However, the inclusion of additional time points revealed an initial decline in TCA cycle activity, followed by a general increase that persists through later age in A-type flies. This differs from C-type flies, where the initially elevated TCA cycle activity showed a general decrease in activity at later ages. Although TCA cycle dysregulation is strongly associated with aging (Sharma and Ramanathan 2020; Borkum 2023), the meaning of the high abundance of TCA cycle intermediary metabolites is difficult to disentangle from metabolomic data alone. High abundances of intermediate metabolites could indicate increased production of them, decreased use, or a combination of the two. Nevertheless, our data shows the pattern of TCA metabolic abundance significantly differs based on the selection regime, with what appears to be a higher degree of coordination found in the A-type populations relative to the C-type populations. Future work incorporating stable isotope tracing could be employed to help elucidate the association between substrate, intermediate, and product metabolites in these pathways of interest.

Conclusion

We set out to investigate the metabolomic signal of accelerated aging associated with selection for early reproduction. We found a high degree of metabolomic convergence between recently derived and long-standing populations of *D. melanogaster* under the same selection regime consistent with other phenotypic convergence previously described in this system. As such, the evolutionary repeatability that defines adaptation in this system also extends to the metabolome. Attempting to use the metabolome as a predictor of age revealed both a general metabolomic signal of aging, and a metabolomic signal of selection regime differences in biological age. Characterizations of metabolomic change associated with selection regime suggest that selection for early reproduction results in significant changes in carbohydrate and amino acid metabolism. More specifically, the response to selection itself appears to be linked to elevated carbohydrate use at early ages to facilitate rapid egg production, potentially at the cost of subsequent glycolytic dysregulation. This work demonstrates the viability of metabolomic phenotyping as a tool for those seeking to use experimental evolution to identify factors underlying complex trait variation.

Figures

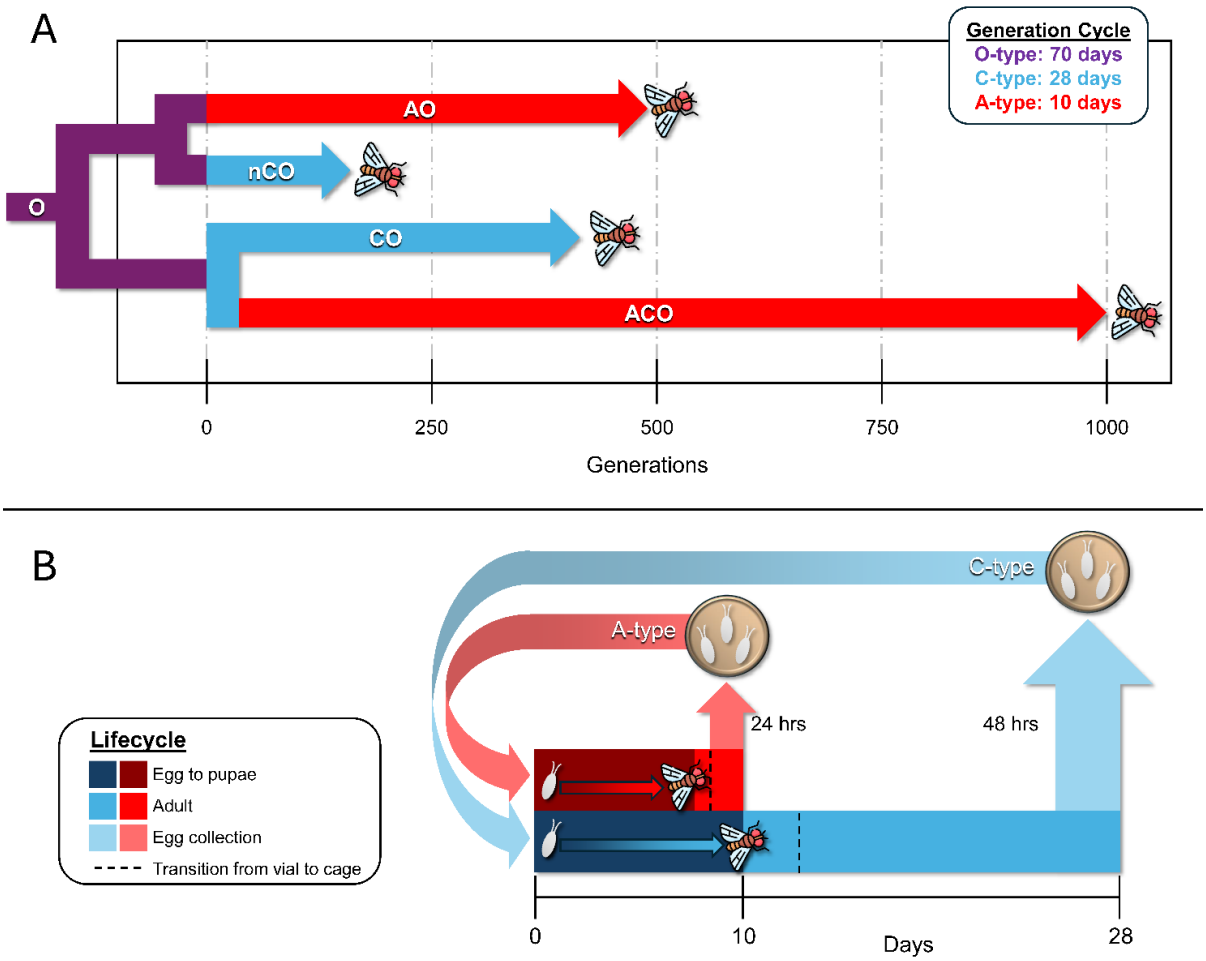

Figure 1. Recent phylogeny and selection regimes for *D. melanogaster* populations of interest. A: Abbreviated diagram of the evolutionary relationship between the populations of interest. The ancestral population for all populations was maintained on a 70-day generation cycle (O-types), both the long-standing (CO) and recently derived (nCO) C-type populations have been maintained on 28-day generation cycles, and both the long-standing (ACO) and recently derived (AO) A-type populations have been maintained on 10-day generation cycles. B: Experimentally controlled reproductive windows, representing two life-history regimes under sustained selection: Accelerated (A) with a 10-day reproductive cycle, and Delayed (C) with a 28-day reproductive cycle. Short reproductive windows, either 24 hours for Accelerated or 48 hours for Delayed, were used to enforce reproductive cycle length.

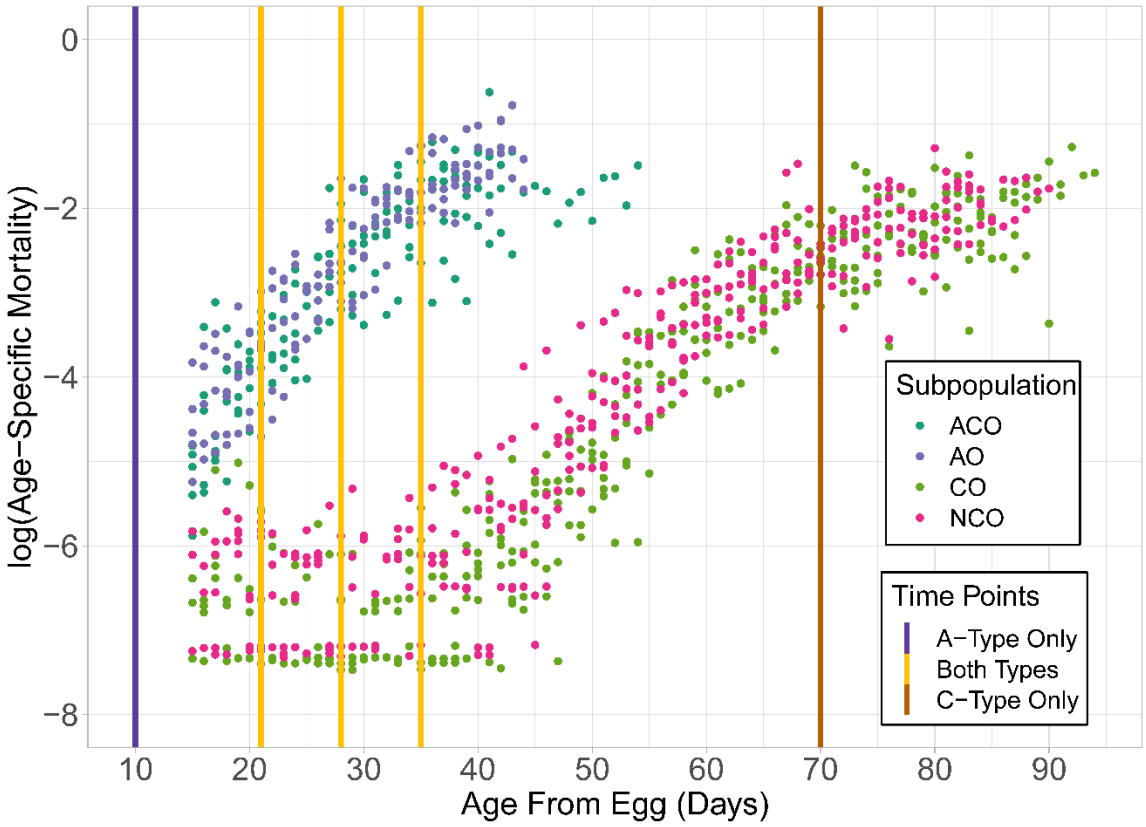

Figure 2. Age-specific mortality and metabolomic sampling design. Female mortality rates for 20 cohorts of A-type (blue and purple) and C-type (pink and green) populations. Recently derived and long-standing subpopulations indicated by color. Each vertical bar represents the collection timepoint in either A-type (blue), C-type (orange) populations, or both (yellow).

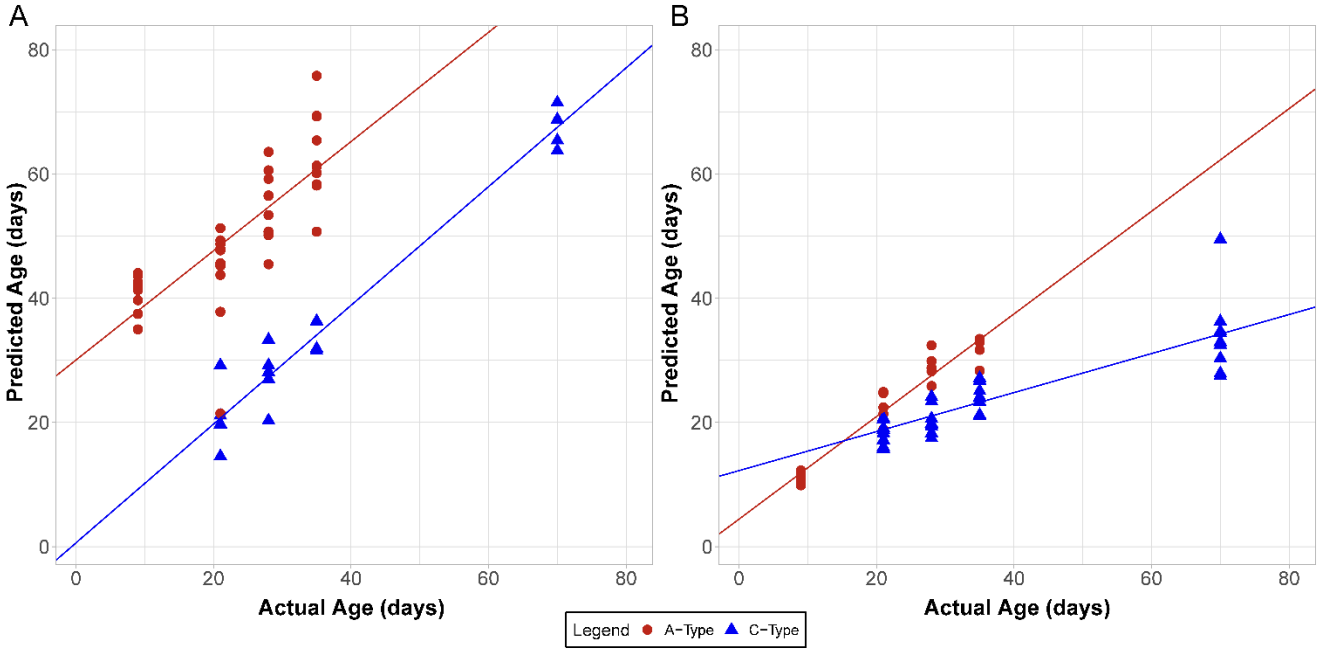

Figure 3. Selection led to different aging trajectories in the metabolome. Predicted age from egg (days) vs chronological age from egg (days) for A-type (red) and C-type (blue) populations based on elastic net models trained on metabolite data from C-type populations (A) or A-type populations (B). Points are predictions from samples held out during training (Methods). The within-regime accuracies of each model were (C-type R^2= 0.955; A-type R^2= 0.886). Lines are the least-squares fits of a linear model (Methods).

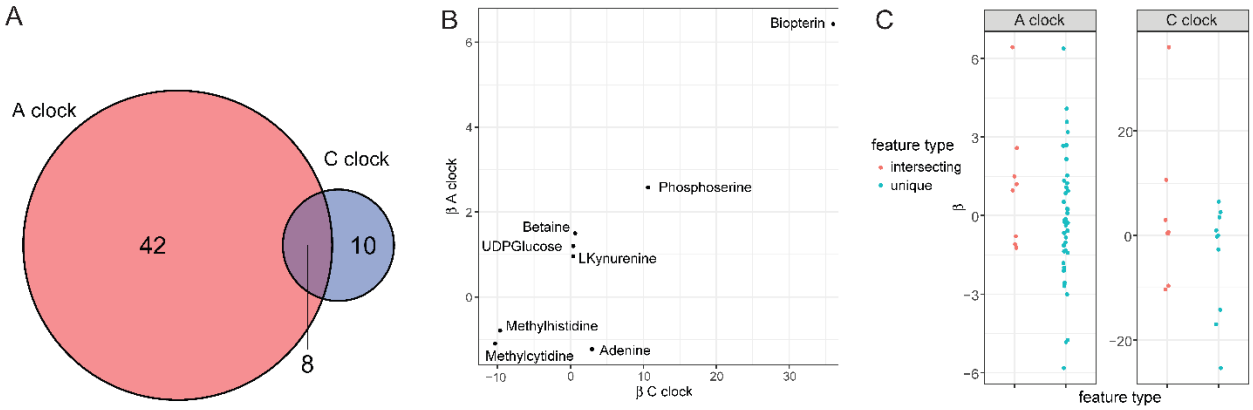

Figure 4. Metabolomic clock features. A: A Venn diagram showing the intersection among the 50 metabolites selected ($\beta \neq 0$) by the A-type clock (red), the 18 selected by the C-type clock (blue), and the 8 selected by both clocks. B: The coefficients (β) fit to each of the 8 metabolites common to the A- and C-type clocks (Pearson's $\rho=0.925$, $P=9.9\times10^{-4}$). C: Comparing the distribution of β fit to metabolites common to both clocks (intersecting) and metabolites unique to each clock. There was not a significant difference in the $|\beta|$ for intersecting and unique metabolites in either clock (Wilcoxon rank sum test, $W \leq 181$, $P>0.74$).

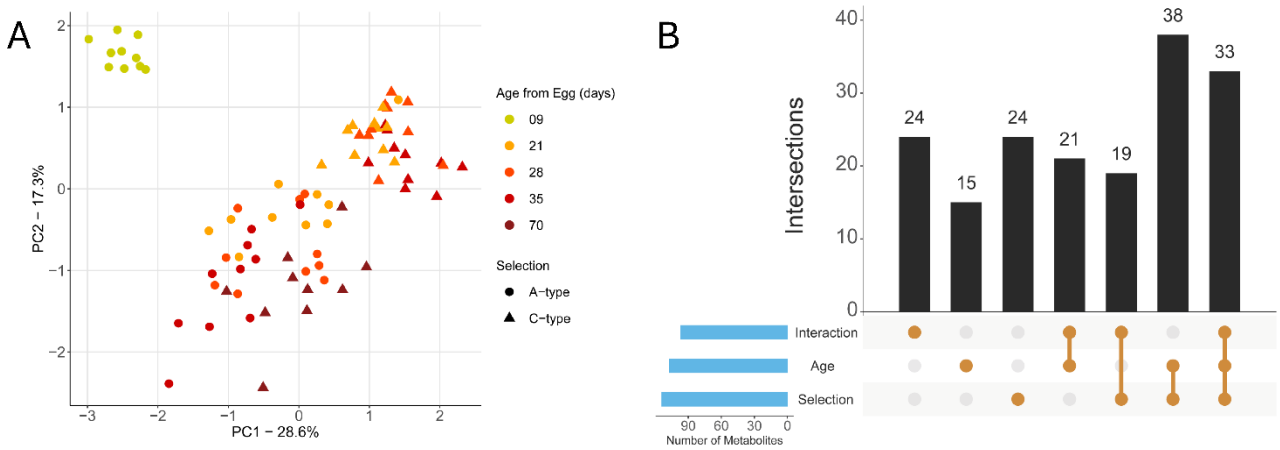

Figure 5. **Differences in metabolite abundance between selection regimes over time.** A: Principal component analysis (PCA) plot shows how samples cluster by Age (from egg, days) and Selection regime based on differences and similarities in relative metabolite abundance along the first principal component (PC1) and the second (PC2). The percentage of variance in the metabolome explained by each PC is shown. B: UpSet plot depicting the number of metabolites that were significant from LMM (FDR <0.01) by each term: Selection, age, and the interaction along the lower left, and the number of metabolites that are significant for each term individually and each combination of terms (Intersections) along the top.

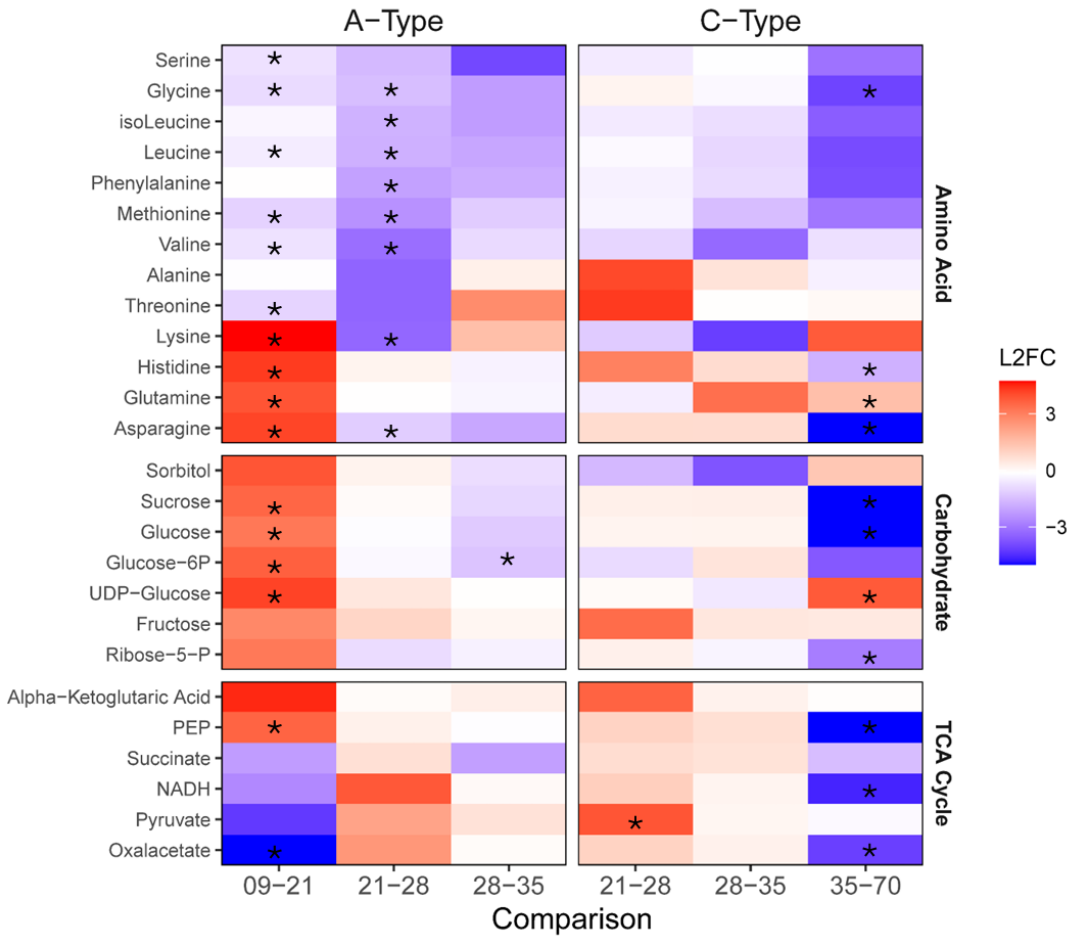

Figure 6. **Altered metabolomic trajectories between selection regimes.** Heatmap shows row-clustering of log2 fold change (L2FC) values of normalized and adjusted metabolite abundance data between ages (days from egg, Comparison) among custom metabolite sets (Amino Acid, Carbohydrate, and TCA Cycle). *Significant values from paired two sample Wilcoxon signed rank test (FDR < 0.05).

Tables

Table 1. Results of the linear mixed-effect model for metabolites of interest.

	Metabolite Subset	Metabolite Name	KEGG ID	Significant LMM Term (FDR <0.01)
A	*Amino Acid 1*	Serine	C00065	Age
		Glycine	C00037	Selection, Age, Interaction
		isoLeucine	C00407	Selection, Age, Interaction
		Leucine	C00123	Selection, Age, Interaction
		Phenylalanine	C00079	Selection, Age, Interaction
		Methionine	C00073	Selection, Age, Interaction
		Valine	C00183	Age, Interaction
	Amino Acid 2	Alanine	C00041	Interaction
		Threonine	C00188	Interaction
	Amino Acid 3	Lysine	C00047	-
		Histidine	C00135	Selection, Interaction
		Glutamine	C00064	Age
		Asparagine	C00152	Selection
B	*Carbohydrate*	Sorbitol	C00794	Interaction
		Sucrose	C00089	Selection, Interaction
		Glucose	C00031	Selection, Age, Interaction
		Glucose-6P	C00092	Selection, Interaction
		UDP-Glucose	C00029	Selection, Age, Interaction
		Fructose	C00095	Age
		Ribose-5-P	C00117	Selection, Age, Interaction
C	*TCA Cycle 1*	Alpha-Ketoglutaric Acid	C00026	Age
		PEP	C00074	Interaction
	TCA Cycle 2	Succinate	C00042	Selection
		NADH	C00004	Interaction
		Pyruvate	C00022	-
		Oxalacetate	C00036	Age

Acknowledgments

This work was supported by the Instrumentation Grant of the National Institutes of Health (NIH S10 OD021562), and by the Nathan Shock Center for Excellence in Basic Biology of Aging (NIH P30 AG013280). The UNCF/Bristol-Myers Squibb E.E. Just Faculty Fund, Career Award at the Scientific Interface (CASI Award) from Burroughs Welcome Fund (BWF) ID # 1021868.01, BWF Ad-hoc Award, NIH Small Research Pilot Subaward to 5R25HL106365-12 from the National Institutes of Health PRIDE Program, DK020593, Vanderbilt Diabetes and Research Training Center for DRTC Alzheimer's Disease Pilot & Feasibility Program. CZI Science Diversity Leadership grant number 2022- 253529 from the Chan Zuckerberg Initiative DAF, an advised fund of Silicon Valley Community Foundation to A.H.J. We thank Dr. Michael Rose at UC Irvine for sharing his experimentally evolved fruit fly populations.

Data Sharing

Raw metabolomic and mortality data are available through Dryad (https://doi.org/10.5061/dryad.1ns1rn92x) and scripts used to process and analyze data are available through Github (https://github.com/mphillips67/A-and-C-Metabolomic-Trajectory-Project).

Author Contributions

M.A.P. conceptualized and oversaw the project. M.A.P., K.R.A., and Z.G.G. designed the experiment. A.P., R.D.R, and V.V.C. collected all fly samples for metabolomics and carried out mortality assays under the supervision of K.R.A. D.D. and D.R. processed samples for metabolomic characterizations. T.B.B. analyzed mortality data. D.L.H, Z.G.G., and B.R.H. analyzed the metabolomic data. D.L.H., A.H. Jr., Z.V., and M.R.M developed possible functional interpretation of metabolomic results. D.L.H., M.A.P, and B.R.H. wrote the manuscript.

References

Alexander, D. L. J., Tropsha, A., & Winkler, D. A. (2015). Beware of R2: Simple, Unambiguous Assessment of the Prediction Accuracy of QSAR and QSPR Models. *Journal of Chemical Information and Modeling*, *55*(7). https://doi.org/10.1021/acs.jcim.5b00206

Austad, S. N., & Fischer, K. E. (2016). Sex Differences in Lifespan. In *Cell Metabolism* (Vol. 23, Issue 6). https://doi.org/10.1016/j.cmet.2016.05.019

Austad, S. N., & Hoffman, J. M. (2018). Is antagonistic pleiotropy ubiquitous in aging biology? *Evolution, Medicine and Public Health*, *2018*(1). https://doi.org/10.1093/emph/eoy033

Avanesov, A. S., Ma, S., Pierce, K. A., Yim, S. H., Lee, B. C., Clish, C. B., & Gladyshev, V. N. (2014). Age- and diet-associated metabolome remodeling characterizes the aging process driven by damage accumulation. *ELife*, *3*. https://doi.org/10.7554/elife.02077

Barghi, N., Tobler, R., Nolte, V., Jakšić, A. M., Mallard, F., Otte, K. A., Dolezal, M., Taus, T., Kofler, R., & Schlötterer, C. (2019). Genetic redundancy fuels polygenic adaptation in Drosophila. *PLoS Biology*, *17*(2). https://doi.org/10.1371/journal.pbio.3000128

Barter, T. T., Greenspan, Z. S., Phillips, M. A., Mueller, L. D., Rose, M. R., & Ranz, J. M. (2019). Drosophila transcriptomics with and without ageing. *Biogerontology*, *20*(5). https://doi.org/10.1007/s10522-019-09823-4

Bates, D., Mächler, M., Bolker, B. M., & Walker, S. C. (2015). Fitting linear mixed-effects models using lme4. *Journal of Statistical Software*, *67*(1). https://doi.org/10.18637/jss.v067.i01

Benjamini, Y., & Hochberg, Y. (1995). Controlling the False Discovery Rate: A Practical and Powerful Approach to Multiple Testing. *Journal of the Royal Statistical Society: Series B (Methodological)*, *57*(1). https://doi.org/10.1111/j.2517-6161.1995.tb02031.x

Borkum, J. M. (2023). The Tricarboxylic Acid Cycle as a Central Regulator of the Rate of Aging: Implications for Metabolic Interventions. In *Advanced Biology* (Vol. 7, Issue 7). https://doi.org/10.1002/adbi.202300095

Bujak, R., Daghir-Wojtkowiak, E., Kaliszan, R., & Markuszewski, M. J. (2016). PLS-based and regularization-based methods for the selection of relevant variables in non-targeted metabolomics data. *Frontiers in Molecular Biosciences*, *3*(JUL). https://doi.org/10.3389/fmolb.2016.00035

Burke, M. K., Barter, T. T., Cabral, L. G., Kezos, J. N., Phillips, M. A., Rutledge, G. A., Phung, K. H., Chen, R. H., Nguyen, H. D., Mueller, L. D., & Rose, M. R. (2016). Rapid divergence and convergence of life-history in experimentally evolved Drosophila melanogaster. *Evolution; International Journal of Organic Evolution*, *70*(9). https://doi.org/10.1111/evo.13006

Carnes, M. U., Campbell, T., Huang, W., Butler, D. G., Carbone, M. A., Duncan, L. H., Harbajan, S. v., King, E. M., Peterson, K. R., Weitzel, A., Zhou, S., & Mackay, T. F. C. (2015). The genomic basis of postponed senescence in Drosophila melanogaster. *PLoS ONE*, *10*(9). https://doi.org/10.1371/journal.pone.0138569

Carvalho-Santos, Z., Cardoso-Figueiredo, R., Elias, A. P., Tastekin, I., Baltazar, C., & Ribeiro, C. (2020). Cellular metabolic reprogramming controls sugar appetite in Drosophila. *Nature Metabolism*, *2*(9). https://doi.org/10.1038/s42255-020-0266-x

Cavigliasso, F., Savary, L., Spangenberg, J. E., Gallart-Ayala, H., Ivanisevic, J., & Kawecki, T. J. (2023). Experimental evolution of metabolism under nutrient restriction: enhanced amino acid catabolism and a key role of branched-chain amino acids. *Evolution Letters*, *7*(4). https://doi.org/10.1093/evlett/qrad018

Charlesworth, B. (1980). Evolution in age-structured populations. *Evolution in Age-Structured Populations.* https://doi.org/10.2307/4092

Chippindale, A. K., Alipaz, J. A., Chen, H. W., & Rose, M. R. (1997). Experimental evolution of accelerated development in Drosophila. 1. Developmental speed and larval survival. *Evolution*, *51*(5). https://doi.org/10.1111/j.1558-5646.1997.tb01477.x

Conway, J. R., Lex, A., & Gehlenborg, N. (2017). UpSetR: An R package for the visualization of intersecting sets and their properties. *Bioinformatics*, *33*(18). https://doi.org/10.1093/bioinformatics/btx364

Dettmer, K., Aronov, P. A., & Hammock, B. D. (2007). Mass spectrometry-based metabolomics. In *Mass Spectrometry Reviews* (Vol. 26, Issue 1). https://doi.org/10.1002/mas.20108

Fabian, D. K., Garschall, K., Klepsatel, P., Santos-Matos, G., Sucena, É., Kapun, M., Lemaitre, B., Schlötterer, C., Arking, R., & Flatt, T. (2018). Evolution of longevity improves immunity in Drosophila. In *Evolution Letters* (Vol. 2, Issue 6). https://doi.org/10.1002/evl3.89

Fox, J., & Weisberg, S. (2019). An {R} Companion to Applied Regression, Third Edition. *Thousand Oaks CA: Sage.*, *September 2012*.

Friedman, J., Hastie, T., Tibshirani, R., Balasubramanian Narasimhan, Kenneth Tay, Noah Simon, Junyang Qian, & James Yang. (2023). Package 'glmnet' - Lasso and Elastic-Net Regularized Generalized Linear Models. In *CRAN*.

Graves, J. L., Hertweck, K. L., Phillips, M. A., Han, M. v., Cabral, L. G., Barter, T. T., Greer, L. F., Burke, M. K., Mueller, L. D., Rose, M. R., & Singh, N. (2017). Genomics of parallel experimental evolution in drosophila. *Molecular Biology and Evolution*, *34*(4). https://doi.org/10.1093/molbev/msw282

Greenspan, Z., Barter, T., Phillips, M., Ranz, J., Rose, M., & Mueller, L. (2024). Genomewide architecture of adaptation in experimentally evolved Drosophila characterized by widespread pleiotropy. *Journal of Genetics*, *103*(1), 8.

Hardy, C. M., Burke, M. K., Everett, L. J., Han, M. v., Lantz, K. M., & Gibbs, A. G. (2018). Genome-Wide Analysis of Starvation-Selected Drosophila melanogaster-A Genetic Model of Obesity. *Molecular Biology and Evolution*, *35*(1). https://doi.org/10.1093/molbev/msx254

Harrison, B. R., Wang, L., Gajda, E., Hoffman, E. v., Chung, B. Y., Pletcher, S. D., Raftery, D., & Promislow, D. E. L. (2020). The metabolome as a link in the genotype-phenotype map for peroxide resistance in the fruit fly, Drosophila melanogaster. *BMC Genomics*, *21*(1). https://doi.org/10.1186/s12864-020-6739-1

Hoffman, J. M., Soltow, Q. A., Li, S., Sidik, A., Jones, D. P., & Promislow, D. E. L. (2014). Effects of age, sex, and genotype on high-sensitivity metabolomic profiles in the fruit fly, Drosophila melanogaster. *Aging Cell*, *13*(4). https://doi.org/10.1111/acel.12215

Houtkooper, R. H., Argmann, C., Houten, S. M., Cańto, C., Jeninga, E. H., Andreux, Ṕeńelope A., Thomas, C., Doenlen, R., Schoonjans, K., & Auwerx, J. (2011). The metabolic footprint of aging in mice. *Scientific Reports*, *1*. https://doi.org/10.1038/srep00134

Ives, P. T. (1970). Further Genetic Studies of the South Amherst Population of Drosophila melanogaster. *Evolution*, *24*(3). https://doi.org/10.2307/2406830

Jin, K., Wilson, K. A., Beck, J. N., Nelson, C. S., Brownridge, G. W. G. W., Harrison, B. R., Djukovic, D., Raftery, D., Brem, R. B., Yu, S., Drton, M., Shojaie, A., Kapahi, P., & Promislow, D. (2020). Genetic and metabolomic architecture of variation in diet restriction-mediated lifespan extension in Drosophila. *PLoS Genetics*, *16*(7). https://doi.org/10.1371/journal.pgen.1008835

Jylhävä, J., Pedersen, N. L., & Hägg, S. (2017). Biological Age Predictors. In *EBioMedicine* (Vol. 21). https://doi.org/10.1016/j.ebiom.2017.03.046

Kezos, J. N., Barter, T. T., Phillips, M. A., Cabral, L. G., Greenspan, Z. S., Arnold, K. R., Azatian, G., Buenrostro, J., Bhangoo, P. S., Khong, A., Reyes, G. T., Rahman, A., Humphrey, L. A., Bradley, T. J., Mueller, L. D., & Rose, M. R. (2023). Building Bridges from Genome to Physiology Using Machine Learning and Drosophila Experimental Evolution. *Physiological and Biochemical Zoology*, *96*(3). https://doi.org/10.1086/724827

Kezos, J. N., Phillips, M. A., Thomas, M. D., Ewunkem, A. J., Rutledge, G. A., Barter, T. T., Santos, M. A., Wong, B. D., Arnold, K. R., Humphrey, L. A., Yan, A., Nouzille, C., Sanchez, I., Cabral, L. G., Bradley, T. J., Mueller, L. D., Graves, J. L., & Rose, M. R. (2019). Genomics of Early Cardiac Dysfunction and Mortality in Obese Drosophila melanogaster. *Physiological and Biochemical Zoology : PBZ*, *92*(6). https://doi.org/10.1086/706099

Koliada, A., Gavrilyuk, K., Burdylyuk, N., Strilbytska, O., Storey, K. B., Kuharskii, V., Lushchak, O., & Vaiserman, A. (2020). Mating status affects Drosophila lifespan, metabolism and antioxidant system. *Comparative Biochemistry and Physiology -Part A : Molecular and Integrative Physiology*, *246*. https://doi.org/10.1016/j.cbpa.2020.110716

Kurup, K., Matyi, S., Giles, C. B., Wren, J. D., Jones, K., Ericsson, A., Raftery, D., Wang, L., Promislow, D., Richardson, A., & Unnikrishnan, A. (2021). Calorie restriction prevents age-related changes in the intestinal microbiota. *Aging*, *13*(5). https://doi.org/10.18632/aging.202753

Kv¥lseth, T. O. (1985). Cautionary note about r2. *American Statistician*, *39*(4). https://doi.org/10.1080/00031305.1985.10479448

Lassen, J. K., Wang, T., Nielsen, K. L., Hasselstrøm, J. B., Johannsen, M., & Villesen, P. (2023). Large-Scale metabolomics: Predicting biological age using 10,133 routine untargeted LC–MS measurements. *Aging Cell*, *22*(5). https://doi.org/10.1111/acel.13813

Laye, M. J., Tran, V., Jones, D. P., Kapahi, P., & Promislow, D. E. L. (2015). The effects of age and dietary restriction on the tissue-specific metabolome of Drosophila. *Aging Cell*, *14*(5). https://doi.org/10.1111/acel.12358

Lu, A. T., Fei, Z., Haghani, A., Robeck, T. R., Zoller, J. A., Li, C. Z., Lowe, R., Yan, Q., Zhang, J., Vu, H., Ablaeva, J., Acosta-Rodriguez, V. A., Adams, D. M., Almunia, J., Aloysius, A., Ardehali, R., Arneson, A., Baker, C. S., Banks, G., … Horvath, S. (2023). Universal DNA methylation age across mammalian tissues. *Nature Aging*, *3*(9). https://doi.org/10.1038/s43587-023-00462-6

Luckinbill, L. S., Arking, R., Clare, M. J., Cirocco, W. C., & Buck, S. A. (1984). Selection for Delayed Senescence in Drosophila melanogaster. *Evolution*, *38*(5). https://doi.org/10.2307/2408433

Ma, S., Avanesov, A. S., Porter, E., Lee, B. C., Mariotti, M., Zemskaya, N., Guigo, R., Moskalev, A. A., & Gladyshev, V. N. (2018). Comparative transcriptomics across 14 Drosophila species reveals signatures of longevity. *Aging Cell*, *17*(4). https://doi.org/10.1111/acel.12740

MacKay, T. F. C., Richards, S., Stone, E. A., Barbadilla, A., Ayroles, J. F., Zhu, D., Casillas, S., Han, Y., Magwire, M. M., Cridland, J. M., Richardson, M. F., Anholt, R. R. H., Barrón, M., Bess, C., Blankenburg, K. P., Carbone, M. A., Castellano, D., Chaboub, L., Duncan, L., … Gibbs, R. A. (2012). The Drosophila melanogaster Genetic Reference Panel. *Nature*, *482*(7384). https://doi.org/10.1038/nature10811

Meador, J. P., Bettcher, L. F., Ellenberger, M. C., & Senn, T. D. (2020). Metabolomic profiling for juvenile Chinook salmon exposed to contaminants of emerging concern. *Science of the Total Environment*, *747*. https://doi.org/10.1016/j.scitotenv.2020.141097

Meyer, D. H., & Schumacher, B. (2024). Aging clocks based on accumulating stochastic variation. *Nature Aging*. https://doi.org/10.1038/s43587-024-00619-x

Mueller, L. D., Rauser, C. L., & Rose, M. R. (2011). Does Aging Stop? In *Does Aging Stop?* https://doi.org/10.1093/acprof:oso/9780199754229.001.0001

Oka, M., Suzuki, E., Asada, A., Saito, T., Iijima, K. M., & Ando, K. (2021). Increasing neuronal glucose uptake attenuates brain aging and promotes life span under dietary restriction in Drosophila. *IScience*, *24*(1). https://doi.org/10.1016/j.isci.2020.101979

Parrott, B. B., & Bertucci, E. M. (2019). Epigenetic Aging Clocks in Ecology and Evolution. In *Trends in Ecology and Evolution* (Vol. 34, Issue 9). https://doi.org/10.1016/j.tree.2019.06.008

Patti, G. J., Yanes, O., & Siuzdak, G. (2012). Innovation: Metabolomics: the apogee of the omics trilogy. In *Nature Reviews Molecular Cell Biology* (Vol. 13, Issue 4). https://doi.org/10.1038/nrm3314

Phillips, M. A., Arnold, K. R., Vue, Z., Beasley, H. K., Garza-Lopez, E., Marshall, A. G., Morton, D. J., McReynolds, M. R., Barter, T. T., & Hinton, A. (2022). Combining Metabolomics and Experimental Evolution Reveals Key Mechanisms Underlying Longevity Differences in Laboratory Evolved Drosophila melanogaster Populations. *International Journal of Molecular Sciences*, *23*(3). https://doi.org/10.3390/ijms23031067

Rodrigues, M. A., Dauphin-Villemant, C., Paris, M., Kapun, M., Mitchell, E. D., Kerdaffrec, E., & Flatt, T. (2023). Germline proliferation trades off with lipid metabolism in *Drosophila*. *Evolution Letters*. https://doi.org/10.1093/evlett/qrad059

Rose, M., & Charlesworth, B. (1980). A test of evolutionary theories of senescence. *Nature*, *287*(5778). https://doi.org/10.1038/287141a0

Rose, M., Passananti, H., & Matos, M. (2010). Methuselah Flies - A Case Study in the Evolution of Aging. In *Methuselah Flies - A Case Study in the Evolution of Aging*. https://doi.org/10.1142/9789812567222

Rose, M. R. (1984). Laboratory Evolution of Postponed Senescence in Drosophila melanogaster. *Evolution*, *38*(5). https://doi.org/10.2307/2408434

Rose, M. R., & Charlesworth, B. (1981). Genetics of life history in Drosophila melanogaster. II. Exploratory selection experiments. *Genetics*, *97*(1). https://doi.org/10.1093/genetics/97.1.187

Rose, M. R., Rauser, C. L., Benford, G., Matos, M., & Mueller, L. D. (2007). Hamilton's forces of natural selection after forty years. In *Evolution* (Vol. 61, Issue 6). https://doi.org/10.1111/j.1558-5646.2007.00120.x

Sarup, P., Pedersen, S. M. M., Nielsen, N. C., Malmendal, A., & Loeschcke, V. (2012). The Metabolic Profile of Long-Lived Drosophila melanogaster. *PLoS ONE*, *7*(10). https://doi.org/10.1371/journal.pone.0047461

Sharma, R., & Ramanathan, A. (2020). The Aging Metabolome—Biomarkers to Hub Metabolites. In *Proteomics* (Vol. 20, Issues 5–6). https://doi.org/10.1002/pmic.201800407

Team, R. C. (2023). R Core Team 2023 R: A language and environment for statistical computing. R foundation for statistical computing. https://www.R-project.org/. *R Foundation for Statistical Computing*.

Tobler, R., Hermisson, J., & Schlötterer, C. (2015). Parallel trait adaptation across opposing thermal environments in experimental Drosophila melanogaster populations. *Evolution*, *69*(7). https://doi.org/10.1111/evo.12705

Turner, T. L., Stewart, A. D., Fields, A. T., Rice, W. R., & Tarone, A. M. (2011). Population-based resequencing of experimentally evolved populations reveals the genetic basis of body size variation in Drosophila melanogaster. *PLoS Genetics*, *7*(3). https://doi.org/10.1371/journal.pgen.1001336

Wang, R., Yin, Y., Li, J., Wang, H., Lv, W., Gao, Y., Wang, T., Zhong, Y., Zhou, Z., Cai, Y., Su, X., Liu, N., & Zhu, Z. J. (2022). Global stable-isotope tracing metabolomics reveals system-wide metabolic alternations in aging Drosophila. *Nature Communications*, *13*(1). https://doi.org/10.1038/s41467-022-31268-6

Weimer, S., Priebs, J., Kuhlow, D., Groth, M., Priebe, S., Mansfeld, J., Merry, T. L., Dubuis, S., Laube, B., Pfeiffer, A. F., Schulz, T. J., Guthke, R., Platzer, M., Zamboni, N., Zarse, K., & Ristow, M. (2014). D-Glucosamine supplementation extends life span of nematodes and of ageing mice. *Nature Communications*, *5*. https://doi.org/10.1038/ncomms4563

Wickham, H. (2016). ggplot2 Elegant Graphics for Data Analysis (Use R!). *Springer*.

Williams, G. C. (1957). Pleiotropy, Natural Selection, and the Evolution of Senescence. *Evolution*, *11*(4). https://doi.org/10.2307/2406060

Zhao, X., Golic, F. T., Harrison, B. R., Manoj, M., Hoffman, E. v., Simon, N., Johnson, R., MacCoss, M. J., McIntyre, L. M., & Promislow, D. E. L. (2022). The metabolome as a biomarker of aging in Drosophila melanogaster. *Aging Cell*, *21*(2). https://doi.org/10.1111/acel.13548

Zou, H., & Hastie, T. (2005). Regularization and variable selection via the elastic net. *Journal of the Royal Statistical Society. Series B: Statistical Methodology*, *67*(2). https://doi.org/10.1111/j.1467-9868.2005.00503.x